metals

Article

Effect of Temperature on the Morphology and Corrosion Resistance of Modified Boron Nitride Nanosheets Incorporated into Steel Phosphate Coating

Mustafa Muhammad *, Ruina Ma, An Du, Yongzhe Fan *, Xue Zhao, Niu Jun and Xiaoming Cao *

Key Laboratory for New Type of Functional Materials in Hebei Province, Tianjin Key Laboratory Material Laminating Fabrication and Interface, Tianjin Engineering and Technology Centre for Environmental-Friendly Coating on Pipeline, School of Materials Science and Engineering, Hebei University of Technology, Tianjin 300132, China
* Correspondence: engrmustafabhatti356@yahoo.com (M.M.); fyz@hebut.edu.cn (Y.F.); gd_sam@galvanize.com.cn (X.C.)

Abstract: In this study, the impact of various temperatures (25 °C, 45 °C, and 55 °C) on q235 steel specimens was studied to analyze the influence on the morphology and corrosion resistance of modified boron nitride nanosheets incorporated into the phosphate coating. The morphology and surface modification of the coating were characterized by scanning electron microscopy (SEM) and Fourier transform infrared spectroscopy (FTIR). SEM results showed that the S-45 steel sample produced a higher number of nucleation sites and reduced grain size with a denser, more robust, and more corrosion-resistant phosphate coating compared to the S-25 and S-55 samples, respectively. The potentiodynamic polarization results demonstrate that the S-45 steel sample exhibited the best corrosion resistance performance with an electric current density of 5.48×10^{-8} A/cm^2, an order of magnitude lower than the S-25 and S-55 samples, respectively. The coating weight results showed that the S-45 steel specimen achieved the densest and most uniform coating (32.14 g/m^2).

1. Introduction

Chemical conversion coatings such as chromate, phosphate, and molybdate are widely utilized in the automotive industry for the preliminary treatment of metallic substrates to improve the adhesion of organic coatings and provide resistance to lubrication, insulation, and corrosion [1–4]. Zinc phosphating is an environmentally friendly surface pretreatment for automotive and structural steel sheets among various coatings due to its high adhesion, lubricity, ease of formation [5], and fast applicability [6,7]. However, the porous structure of phosphate coatings compromises their corrosion resistance [8]. Corrosion resistance is significantly affected by parameters such as coating thickness, porosity, and microstructure. It has been noted that increasing the thickness and decreasing the porosity of the coating are instrumental in obtaining the desired corrosion resistance. Unfortunately, various zinc phosphate coatings still have limitations in terms of thickness, which poses another challenge [9].

Investigations were carried out to enhance the corrosion resistance of phosphate coatings by changing reaction time, temperature, or accelerators and incorporating metallic ions in the phosphating bath [10]. Additionally, the selection and quantity of accelerators were considered essential variables for the ultimate coating efficiency. However, the temperature and immersion time of the zinc phosphating bath significantly influence the performance and durability of the phosphate coating applied to steel [11]. The deposition and development of zinc phosphate crystals may be inhibited if the phosphating bath temperature is not maintained within the required range, leading to a weaker coating with poor coverage

and reduced corrosion resistance. It occurs because, at higher temperatures, the soluble primary zinc phosphate is more likely to transform into the insoluble tertiary zinc phosphate, forming a thin coating on the metal surface and preventing further deposition and the development of crystals.

Similarly, the formation process of coatings may be prolonged due to the absence of preliminary tertiary phosphates when the temperature is excessively high (>60 °C). In order to achieve the most effective phosphate coating, it is essential to maintain the bath temperature (<60 °C) to sustain equilibrium between primary and tertiary phosphates [5]. The operational temperature significantly influences the morphology and characteristics of the phosphate coating [12]. Khalid Abdalla et al. examined the effects of phosphating temperature on the surface texture and anti-corrosive properties of zinc phosphate coating on mild steel at variant temperatures to deposit phosphate coating on steel [5].

Similarly, the effects of different phosphate solution temperatures and phosphate time immersions on the Zn–Ca phosphate coating with PTFE on the surface of 45 steel were studied by Zhang et al. through the dipping method. It was concluded that the optimum conditions for coating thickness and PTFE particle content were achieved at a phosphate solution temperature of 65 °C. The elevated temperature accelerates hydrolysis and crystallization reactions, increasing the coating formation rate and improving coating thickness [13].

Furthermore, employing an accelerator could effectively improve the performance of phosphate coatings by speeding up the phosphating process and lowering the operating temperature [14]. Shibli et al. demonstrated that phosphate coatings developed at 55 °C in the presence of nano-TiO_2 on galvanized steel produced larger crystals and better surface adhesion with improved protective properties against corrosion [15]. Similarly, M. Arthanareeswari et al. studied that nano-TiO_2-incorporated nano zinc phosphate coatings were synthesized as accelerators at low temperatures of 27 °C on mild steel substrates, resulting in a bigger coating weight, a reduction in the crystal size, and an amplified coverage of the surface. However, although low-temperature phosphating baths are preferred over high-temperature ones due to the increased energy expenditure, low-temperature bathing operations are tedious and must be accelerated by some agent [16]. Currently, two-dimensional (2D) nanomaterials are being utilized as accelerators, such as graphene oxide (GO) [14], boron nitride (BN) [17], modified boron nitride (PDA@BN) [10], and MoS_2 [18]. These nanomaterials help reduce the phosphating process's conventional time and operating temperatures below 98 °C with increased coating mass and corrosion resistance [19,20]. Xie et al. investigated fast, low-temperature processing at 45 °C to formulate a zinc phosphate coating on steel augmented with GO to constitute evenly dense coatings with exceptional corrosion protection [14]. Nevertheless, the energy consumption and lack of environmentally friendly features make it challenging to be employed in industrial operations.

The extraordinary properties of nanomaterials, mainly hexagonal boron nitride (h-BN), have attracted significant attention due to their diverse applications [10,21]. These properties include high thermal stability, resistance to degradation, mechanical strength, and biochemical inertness, enabling their application in numerous industries [22]. However, the challenges presented by h-BNs are their larger particle size, lack of dispersion ability, and a tendency for the boron nitride to cluster, which can limit its anticorrosion properties [10]. Therefore, this study utilized boron nitride modified by polydopamine (BN@PDA) nanosheets to produce phosphate coatings on mild steel. However, the microporous nature of the phosphate coating has compromised its corrosion resistance. Silane coatings, which result in better sealing properties than phosphate-based coatings with enhanced protection against corrosive media, have been demonstrated to improve corrosion resistance in numerous eco-friendly pretreatments containing organo-silane surfaces, such as KH560 [23]. Polydopamine (PDA) was utilized to improve the diffusion and alteration of a chemical bonding interface between silane (KH560) and a phosphate coating on a boron nitride surface.

This study investigates the impact of temperatures (25 °C, 45 °C, and 55 °C) on boron nitride modified by poly(dopamine) phosphate coatings on mild steel. Scanning electron microscopy (SEM) and Fourier transform infrared spectroscopy (FTIR) are employed to characterize BN@PDA-phosphate coatings. Scanning electron microscopy (SEM) and energy dispersive spectroscopy (EDS) also examine the surface morphology of phosphate coatings deposited on steel at varying temperatures. The corrosion resistance of the phosphate coatings was studied by polarization curve and electrochemical impedance spectroscopy (EIS) in a 3.5% NaCl solution.

2. Materials and Methods

2.1. Materials

Q235 steel substrates (40 mm × 40 mm × 3 mm) with chemical compositions of C: 0.22; S: 0.05; Si: 0.35; P: 0.05; Mn: 1.40; Fe: balance were utilized for zinc phosphating experiments. The zinc phosphating bath composition employed in this study was: H_3PO_4 85% (3.0 g/L), H_3PO_3 99% (2.0 g/L), KH560 (Silane) 3-glycodyloxypropyltrimethoxysilane (1.50 g/L), Zn $(NO_3)_2 \cdot 6H_2O$ (80 g/L), Zn $(H_2PO_4)_2 \cdot 2H_2O$ (50 g/L), PDA@BN (0.6 g/L), and (10.0 wt.%) NaOH, respectively. All the chemicals in this experiment were of empirical grade and utilized without additional purification.

2.2. Zinc Phosphating Treatment Procedure

Firstly, steel samples were finely ground and polished, followed by immersion into a zinc phosphating bath and ultra-sonication for 30 min to ensure the uniform distribution of polydopamine-modified boron nitride and phosphating solution. The steel samples were then submerged in a bath and maintained at the desired temperature for a specific time. The concentration of modified boron nitride used in the zinc phosphating bath was 0.6 g/L at varying temperatures, which were denoted as S-25 (25 °C), S-45 (45 °C), and S-55 (55 °C). Similarly, the baths without adding modified boron nitride at these temperatures were denoted as pure 25, pure 45, and pure 55, respectively. The samples exhibited the formation of a grey coating with distinct, bright crystalline regions. After phosphating, the samples were washed with distilled water to eliminate any residual acid or dissolved salts. Subsequently, the specimens were dried in compressed air at ambient temperature to facilitate further analysis.

2.3. Synthesis of BN@PDA

The synthesis of h-BN@PDA was carried out in accordance with preceding reports in the literature [10]. Two-dimensional h-BN nanosheets (0.6 g) were added to a solution of Tris (hydroxyethyl amino-methane) (0.16 g) and then subjected to ultrasonic waves for 30 min. Subsequently, the solution was accompanied by an addition of 30 milliliters (mL) of ethanol and dopamine hydrochloride, weighing 0.24 g. The mixture was then continuously agitated at a temperature of 60 °C for 6 h to enhance the dispersibility of the BNs nanosheets and reduce the polymerization rate of poly(dopamine) to prevent the aggregation of BNs.

2.4. Surface Characterization

The surface morphology and structure of zinc phosphate coatings were studied using scanning electron microscopy (SEM) (JSM-06510A, JEOL, Tokyo, Japan) with a 20.0 kV acceleration voltage. The coating weight determination of the phosphate coatings was according to the formula $W = \frac{W1 - W2}{A}$. In this formula, W is the phosphate coating weight per unit area, W1 is the sample weight after phosphating, W2 is the sample weight after the coating was removed, and A is the surface area of the phosphate sample [24]. A specifically formulated solution was used to analyze a steel sample's phosphate coating. Upon immersion of the specimen in the solution containing 12% Na_2EDTA, 4% triethanolamine, and 9% NaOH at a temperature of 70 °C for 5 min, the coating was dissolved entirely, exposing the underlying steel substrate. The processes of pre-dissolving and post-dissolving

of steel specimens, denoted as W1 and W2, respectively, were accompanied by a mass measurement [25].

2.5. Corrosion Performance Evaluation

Polarization curves (Tafel) and electrochemical impedance spectroscopy (EIS) studies were employed to investigate the corrosion resistance performance of phosphate coatings on steel samples. The electrochemical working station CHI660E (Chenhua, Shanghai, China) was utilized. Electrochemical measurements were conducted at room temperature using a 3.5% NaCl solution. The frequency range (FR) utilized for the electrochemical impedance spectroscopy (EIS) measurements was 10 mHz to 100 kHz. A waiting time of 400 s was set before conducting electrochemical impedance spectroscopy (EIS) to ensure a stable open-circuit potential (OCP). The results of the EIS were recorded and evaluated using Echem Zsimp Software Win (Q5; Ann Arbor, MI, USA). The polarization curves were obtained by examining the potentiodynamic polarization ranging from the cathodic to anodic regions ($\pm$300 mV vs. OCP) at a scan rate of 1 mV/s. The electrochemical workstation was connected to a computer with the software CHI660E (Chenhua, Shanghai, China) used for Tafel extrapolation and calculating the corrosion current density, corrosion potential, and electrochemical parameters. The procedure was repeated three times, with the average value used for analysis.

3. Results and Discussion

3.1. Characterization of PDA@BNs Nanosheets

The SEM images in Figure 1a,b depicts the BN and BN@PDA nanosheets, respectively. BN nanosheets, commercially available in round disks, possess strong Van der Waals interactions, having a diameter of 256 nm and a thickness of 34 nm, resulting in a well-flaked and smooth surface structure. However, boron nitride nanosheet research continues; it has often encountered challenges due to its bulky particle size and weak distribution strength. Furthermore, hexagonal boron nitride tends to agglomerate because of its poor blending capabilities with the matrix, and it is not easy to find the BNs' diameter measurement under SEM analysis (Figure 1a) [26,27]. However, the stacked BNs are no longer visible after modification. At the same time, poly(dopamine) particles could be formed on the surface of the BNs nanosheets in the form of smaller, coarser particles.
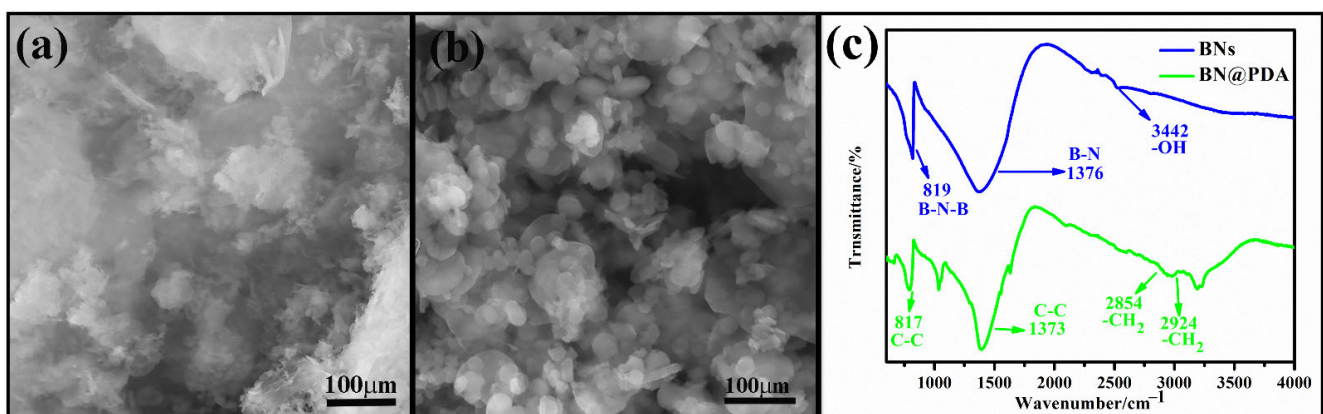

Figure 1. Comparison of SEM images (**a**,**b**) and FTIR spectra (**c**) of BNs (**a**,**c**) and PDA@BNs (**b**,**c**).

Analysis of FTIR demonstrated that poly(dopamine) was successfully used to modify the boron nitride nanosheets. The FTIR spectra of boron nitride (BNs) and h-BN@PDA (poly(dopamine) modified hexagonal boron nitride) are shown in Figure 1c. The in-plane stretching vibration peak and out-of-plane bending vibration peak of B–N are represented by absorption peaks near 1376 cm^{-1} and 819 cm^{-1}, respectively [28]. The Fourier transform infrared spectroscopy of poly(dopamine) modified h-BN demonstrated new absorption

bands at 2924 cm^{-1} and 2854 cm^{-1} corresponding to the –CH$_2$– stretching vibrations. Additionally, the C–C bending vibrations of phenol rings in 1300 cm^{-1} to 1600 cm^{-1}, respectively, were evident [29]. However, due to boron nitride nanosheets (BNs) agglomeration, the size and incompatibility of the boron nitride particles with the phosphating solution restricted their application for anticorrosion performance.

The chemical stability of boron nitride nanosheets, challenging to alter, can be modified by utilizing poly(dopamine), as demonstrated in Figure 2 [30]. The dispersion stability of boron nitride and poly(dopamine)-modified boron nitride nanosheets (0.60 g/L) after 15 min of sonication in a phosphating fluid exhibited white and greyish brown colors, respectively, as shown in Figure 2. However, boron nitride nanosheets (BNs) were precipitated at the bottom of the bath. Nevertheless, the h-BN@PDA particles were well dispersed after 6 h, suggesting that the PDA layers were successfully applied to the BNs nanosheets, as the modified sheets no longer showed compatibility with the phosphating solution.

Figure 2. The dispersion stability of PDA@BN and BN nanosheets (0.60 g/L) in a phosphating bath at 0 and 6 h was examined visually, as shown in the digital photos.

3.2. Morphology of Phosphate Coating

Figure 3a–l depicts the SEM images of the phosphate coating's microstructure at different temperatures after zinc phosphating. The phosphating time was maintained constant during the experiment to examine the impact of bath temperature on phosphate coating quality. However, to study the coating formation, varying times were employed for a better understanding of the morphology of the coating. As shown in Figure 3, the growth of phosphate crystals is accelerated by incorporating modified h-BN nanosheets. There is no noticeable deposition at 25 °C (S-25) after 5 min of immersion, as shown in Figure 3a. At the specified temperature, crystal nucleation occurs slowly, leading to a negligible amount of crystals growing within 20 min (Figure 3c). It suggests that their kinetics are slow, regardless of the low temperature that causes the reactions.

Similar to the S-25 specimen, the pure sample exhibited slower kinetics of crystal development, as demonstrated in Figure 3d. Most of the sample was uncoated after 20 min without any modified boron nitride addition. In contrast, the specimens with modified h-BNs show apparent crystal formation after 20 min of phosphating. As the phosphating process progresses, tiny phosphate crystals cover the substrate. However, phosphate coatings obtained at 45 °C (S-45) have finer and smaller phosphate crystals, leading to a continuous and compact structure (Figure 3g).
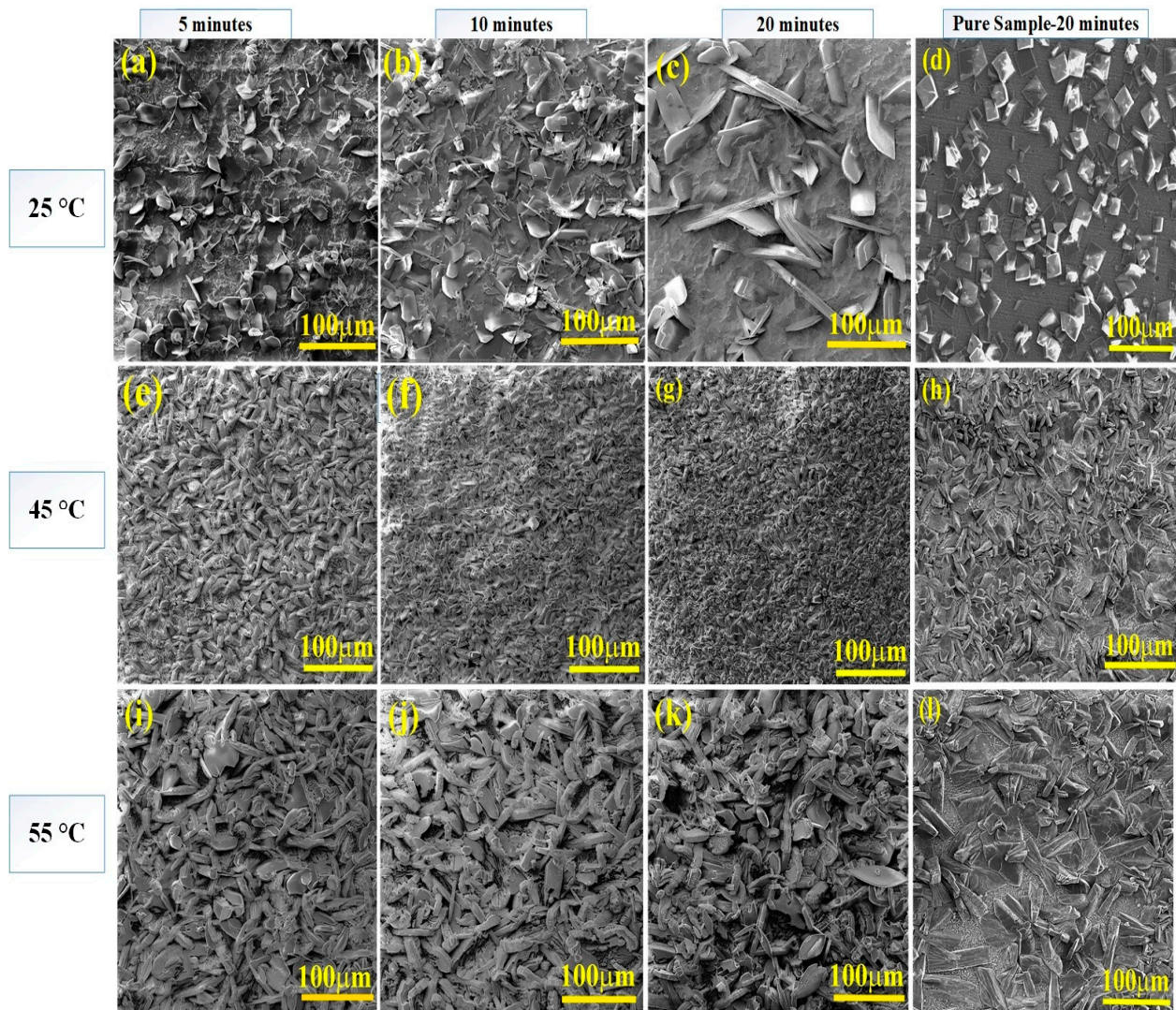
Figure 3. SEM images of phosphate coatings were obtained by different time immersions in a phosphating bath at different coating temperatures (25 °C, 45 °C, and 55 °C, respectively).

At a temperature of 45 °C in a pure sample, the steel specimen exhibits inadequate coating thickness and compactness, with some regions of the sample remaining uncoated, indicating a less compact structure (Figure 3h). A dense coating is observed on the steel surface at a temperature of 55 °C (S-55), leading to phosphate crystal growth (Figure 3k). As depicted in Figure 3l, an increase in phosphating temperature to 55 °C resulted in the formation of larger phosphate crystals, with a significant portion remaining uncoated after 20 min. The reaction kinetics are comparatively high at this temperature. Higher working temperatures result in coarse crystals and a dense coating, which exhibit poor corrosion characteristics [31]. The kinetics of the phosphate coating reaction are enhanced at elevated temperatures, leading to an enhanced deposition rate. Nevertheless, too high temperatures could trigger the rapid transformation of soluble phosphates into their insoluble forms, which dissolve slowly. The excessive presence of insoluble phosphate particles in the coating formulation leads to the formation of thick and coarse layers on the surface, resulting in insufficient coating coverage [5].

As illustrated in Figure 3a–l, it is evident that the advancement of phosphate coating occurs during the early phase of low immersion time [32], and incomplete phosphate coating forms in Figure 3a. As shown in Figure 3c, the phosphate crystals grow with increasing immersion time, and uniform and compact coatings are obtained for the S-25 sample.

The orientation of modified hexagonal boron nitride (h-BN) influences the formation of phosphate crystals and is linked to the resulting structural differences in the crystals. At 45 °C, the crystals for the S-45 sample formed a striped pattern, while those grown for the S-55 sample at 55 °C were flat, plate-like. The crystallization kinetics at these different temperatures have been attributed to the influence of modified h-BNs [10]. Additionally, due to the silane and steel substrate interaction, a consistent and well-distributed silane film was formed, effectively filling the micropores in the phosphate coating. However, it was observed that the PDA@BN accelerated the phosphate coating formation for the S-45 sample and the S-55 sample, developing phosphate crystals all over the specimen with uniform and compact structures.
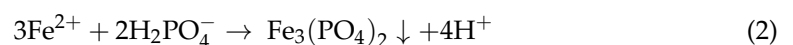
3.3. Formation Mechanism

The phosphating process is a delicate chemical and electrochemical procedure that involves micro-anodic and cathodic terminals. As the steel panel is placed in a phosphating solution, the free phosphoric acid initiates a topochemical reaction, dissolving the iron at the micro-anodes on the substrate [10]. The process also includes reactions between silane and a metallic substrate, hydrolysis of silane, and oxidation–reduction reactions of the accelerators [33]. When the steel substrate is immersed in the phosphating bath, the steel substrate dissolves to form ferrous (iron (II)) (Fe^{2+}) ions, followed by the release of hydrogen (H_2) gas [18].
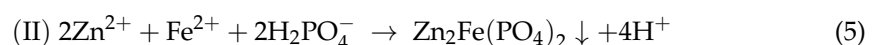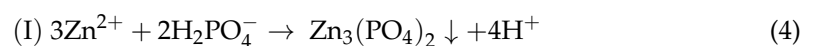
Iron phosphating:
Pickling:

$$3Fe + 6H^+ \rightarrow 3Fe^{2+} + 3H_2 \uparrow \tag{1}$$

Forming of iron phosphate:

$$3Fe^{2+} + 2H_2PO_4^- \rightarrow Fe_3(PO_4)_2 \downarrow + 4H^+ \tag{2}$$

Zinc phosphating:
Pickling:

$$Fe + 2H^+ \rightarrow Fe^{2+} + H_2 \tag{3}$$

$$(I)\ 3Zn^{2+} + 2H_2PO_4^- \rightarrow Zn_3(PO_4)_2 \downarrow + 4H^+ \tag{4}$$

$$(II)\ 2Zn^{2+} + Fe^{2+} + 2H_2PO_4^- \rightarrow Zn_2Fe(PO_4)_2 \downarrow + 4H^+ \tag{5}$$

Based on the coating formation process mentioned above, the following phosphating mechanism for the modified boron nitride nanosheets has been proposed: When the modified boron nitride nanosheets are doped in the phosphating solution, the nanosheets are first adsorbed on the surface of steel due to their high specific surface area, as shown in Figure 3. Similar to GO, modified boron nitride nanosheets can be used as deposition substrates for metallic ion capture (Fe^{2+} and Zn^{2+}) that can promote the dissolution reactions of iron and H_3PO_4 reactions (1) and (2) [14]. The modified h-BN can increase the rate of phosphating, generate insoluble phosphate crystals in untreated conditions, and act as nucleation sites, resulting in a denser and finer phosphate coating on the surface of the steel.

3.4. Phosphate Coating Weight

Steel specimens were submerged in a phosphating bath containing PDA@BN nanosheets for varying times at different temperatures (25 °C, 45 °C, and 55 °C) to assess the integrity and thickness of the phosphate coatings by mass per unit area (MPA). The MPA can be measured by chemically removing the phosphate coatings and calculating the weight loss. The coating was dissolved entirely in the solution at a temperature of 70 °C for 5 min, exposing the underlying steel substrate. A mass measurement accompanied the processes of pre-dissolving and post-dissolving of steel specimens. It was observed that the MPA

shows significant changes at different temperatures. The MPA of the S-25 sample phosphate coating recorded was 25.4 g/m^2.

In contrast, the coating weight of samples S-45 and S-55 increased to 32.14 g/m^2 and 28.49 g/m^2, respectively. The increase in coating weight in the S-55 sample is due to the conversion of primary phosphate to tertiary phosphate before the metal surface has been treated. All measurements were performed three times, and average values were used.

3.5. Elemental Dispersive Spectroscopy Analysis (EDS) of Phosphate Coatings at Different Temperatures

An investigation of the elemental distribution of the phosphate coating was performed utilizing an energy-dispersive spectrometer (EDS) mapping at 20.0 kV. It was performed on the steel specimen surface at 25 °C, 45 °C, and 55 °C temperatures. Figures 4–6 illustrate the resulting surface morphology and elemental distribution. The O and P elements characterize the phosphate salts, with a homogenous occurrence across the substrate, suggesting that the phosphate samples consisted of crystals with varying components and appearances. An increase in concentrations of the Fe element was noted, which may stem from phosphophyllite $Zn_2Fe(PO_4)_2 \cdot 4H_2O$, P–Fe–Zn crystals, or from the steel itself. Since the phosphate coating is porous, the penetration of the electron beam may explain the high readings for Fe. In addition, an increase in Zn^{2+} ion concentrations was observed in the phosphate crystals compared to those at the gaps. Mappings of B, Si, and N elements were also seen on the samples due to the compactness of the phosphate coating. The elemental distribution of the S-25 sample in Figure 4 clearly shows that a significant portion of the sample is uncoated. Only a small number of phosphate crystals are present, similar to the SEM analysis in Figure 3c. However, Si, B, and N mappings appeared on the sample regions, forming a smooth silane film over the sample.

Similarly, the elemental distribution of the S-45 sample in Figure 5 represents that a sample is covered with smaller phosphate crystals covering the entire portion of the specimen with a continuous and compact structure, as evident in SEM analysis (Figure 3g). Fe mappings showed a smaller sample region uncoated, confirming the continuous and uniform coating at the S-45 sample.

The elemental distribution of the S-55 sample in Figure 6 represents bigger phosphate crystals, indicating a densely coated sample, as evident in SEM analysis (Figure 3k).
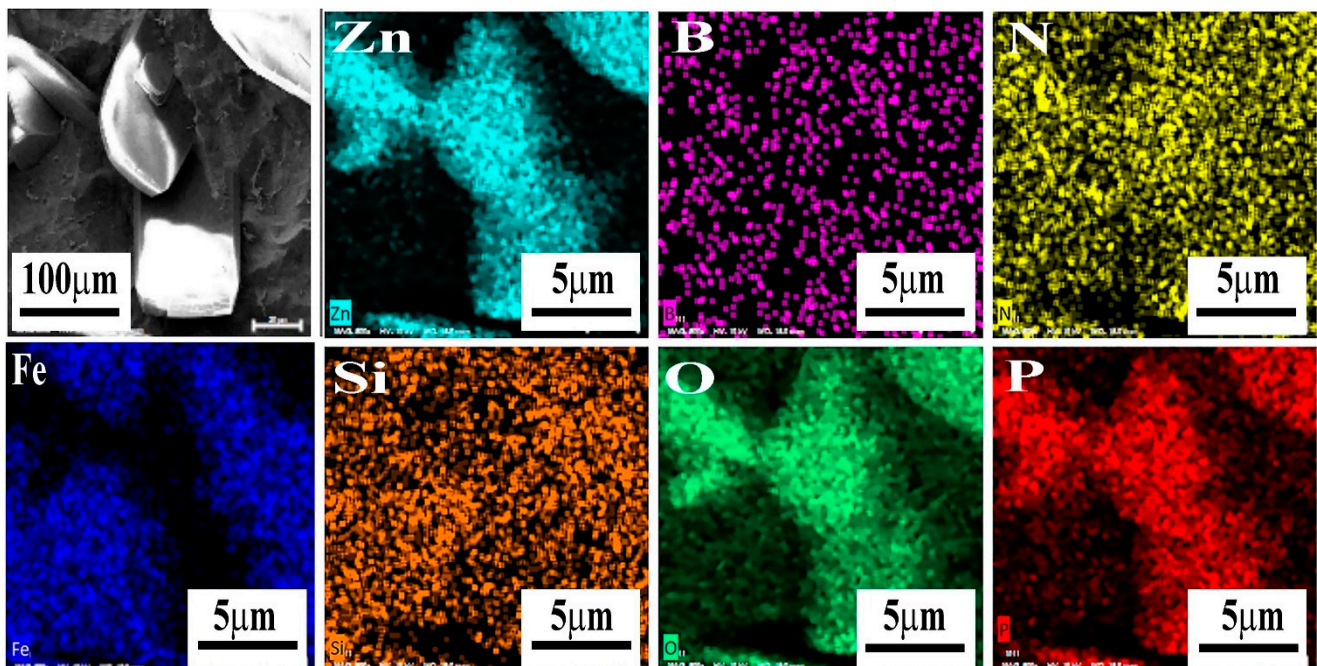

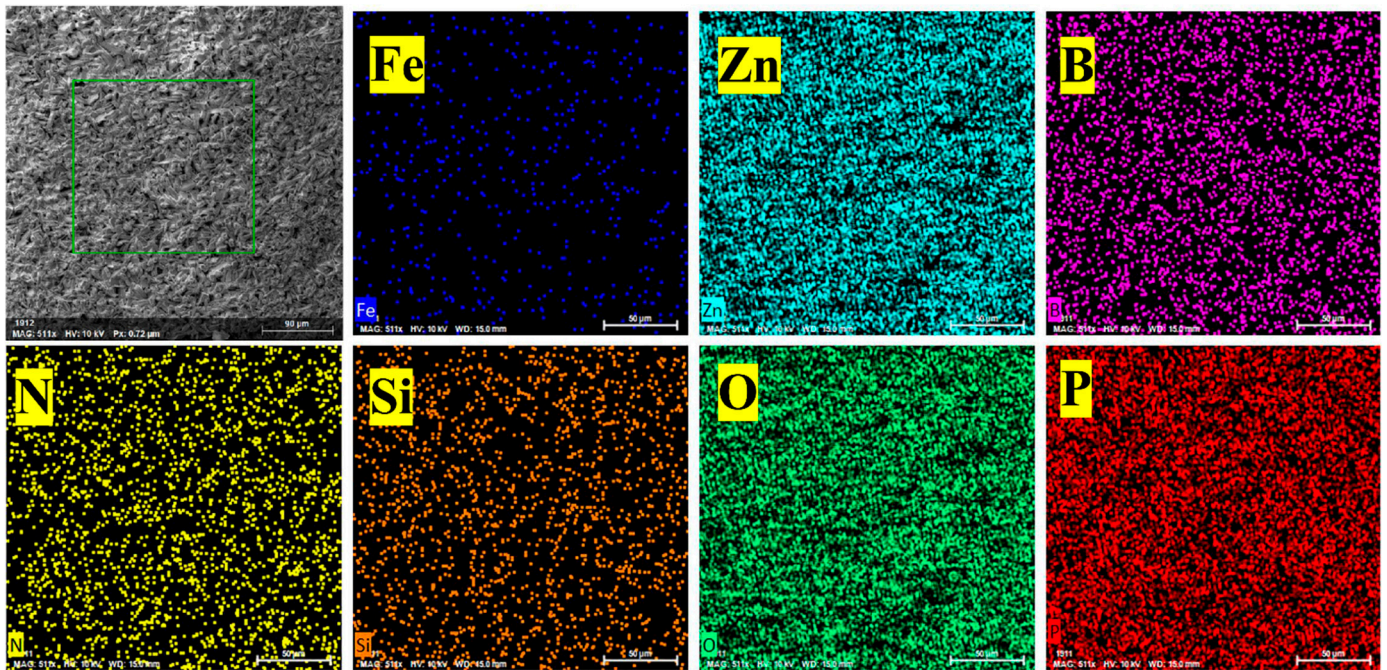**Figure 4.** Elemental analysis of phosphate coating on steel at 25 °C.

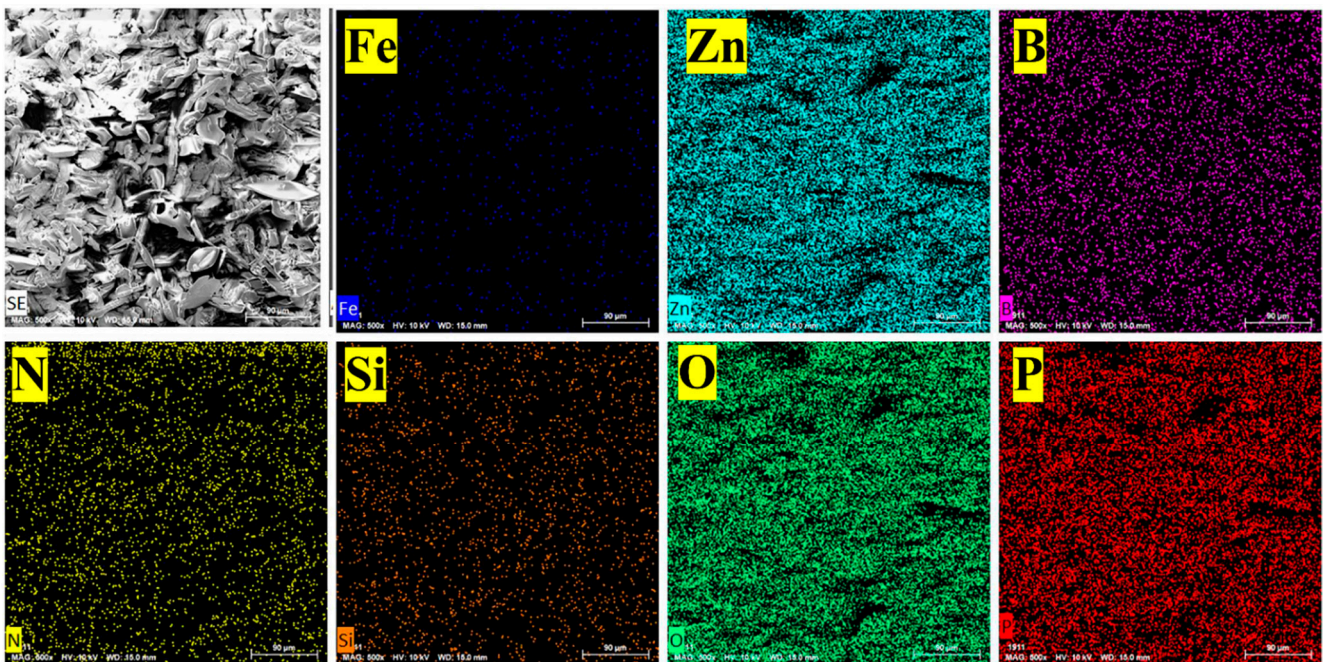**Figure 5.** EDS analysis of phosphate coatings at 45 °C.

Figure 6. EDS mappings of phosphate coating at 55 °C.

3.6. Effect of Temperature on Corrosion Performance

The polarization curves of steel samples coated with phosphate in a 3.5% NaCl solution are presented in Figure 7. Steel surfaces were subjected to 20 min of immersion in a phosphating bath at various temperatures. The accompanying electrochemical data and the corrosion rate of each sample are detailed in Table 1. As demonstrated in Figure 7, steel samples show increased positive corrosion potential, decreased corrosion current density, and higher polarization resistance. These indicate an improvement in the corrosion performance of steel due to phosphating treatment. Table 1 shows that the phosphate coatings prepared for the S-45 sample had the highest polarization resistance and the

lowest corrosion current density, attributed to a thicker, more compact coating layer. It has been suggested that slower reactions during the zinc phosphating process develop more phosphophyllite crystals, as represented in SEM Figure 3a–l. This leads to a thicker phosphate coating layer obtained from coating weight results, increased polarization resistance, and a lower corrosion current density than pure samples at different temperatures. As the operating temperature increases, it is predicted to reduce the amount of phosphophyllite present. The higher the temperature, the more the metal dissolution rate increases [12], leading to larger crystal formations.
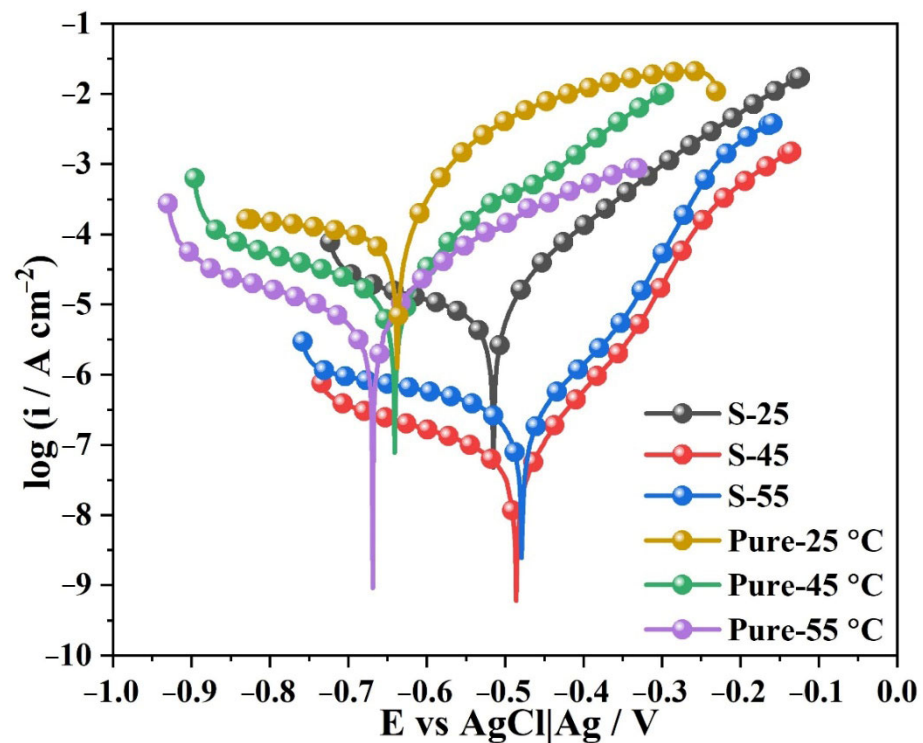

Figure 7. Polarization curves of steel samples received from the phosphating bath at different temperatures.

Table 1. Parameters of the potentiodynamic polarization curves.

Sample	E_{Corr} (V)	i_{Corr} (A/cm^2)	βa (mV/dec^{-1})	$-\beta c$ (mV/dec^{-1})	Corrosion Rate (Mil/Year)	R_p (K$\Omega \cdot$cm^2)
Pure 25 (25 °C)	−0.651	5.78×10^{-6}	10.916	4.347	2.65	4931
Pure 45 (45 °C)	−0.596	1.65×10^{-5}	10.778	3.822	7.59	1801
Pure 55 (55 °C)	−0.630	7.19×10^{-6}	8.776	3.989	3.30	4737
S-25 (25 °C)	−0.528	8.23×10^{-6}	12.547	3.109	3.76	3374
S-45 (45 °C)	−0.454	5.84×10^{-8}	12.324	4.907	26.7	4.315×10^5
S-55 (55 °C)	−0.434	2.32×10^{-7}	11.659	5.382	10.6	1.096×10^5

The Tafel extrapolation method was employed to evaluate the potentiodynamic polarization curves and various electrochemical parameters, including potential (E_{corr}), anodic (βa), and cathodic (βc) slopes, as well as corrosion density, as listed in Table 1. The corrosion potential of the samples containing incorporated modified boron nitride, denoted as S-25, S-45, and S-55, was observed to be positively shifted compared to the untreated samples (Pure) at temperatures of 25 °C, 45 °C, and 55 °C, as depicted in Figure 7. This shift towards a more positive potential indicates an improvement in corrosion resistance.

Furthermore, a high operating temperature produces abundant amounts of insoluble tertiary zinc phosphate and dissolved phosphate acid before treatment of the metal

is conducted [12]. Similarly, the impact of various deposition temperatures on the surface coverage and morphology of modified BNs phosphate coatings on Q235 steel was investigated. The results revealed that an increase in deposition temperature led to the formation of a coarse crystal structure and a heavier coating, adversely affecting the steel's corrosion properties. However, modified h-BN nanosheets were found to significantly decrease the corrosion current density (i_{Corr}) of the coatings, providing excellent anticorrosion performance on phosphate-coated steel. A positive shift in the value of E_{Corr} was observed depending on the durability and weight of the coatings, with the most significant shift occurring on the steel samples coated with modified BNs nanosheets, as shown in Table 1. A reduction of one order of magnitude was seen in the i_{Corr} of the phosphate-coated samples at 45 °C, resulting in a minimum value of 5.84×10^{-8} A/cm^2.

3.7. Electrochemical Impedance Spectroscopy (EIS)

Electrochemical impedance analysis evaluated the phosphate coating's anti-corrosive performance on the zinc-phosphate steel. EIS measurements were conducted on pure 25, pure 45, pure 55, S-25, S-45, and S-55 samples, with the results displayed in Figure 8a–c as Nyquist, Bode, and phase angle graphs, respectively. The impedance was measured in a 3.5% NaCl solution at the open circuit potential. An investigation was carried out to evaluate the anti-corrosive properties of zinc phosphate coatings on steel specimens treated with modified hexagonal boron nitride (h-BN) nanosheets compared to untreated samples employing Zsimpwin software. This enables a comprehensive analysis of the electrochemical behavior of the coatings and corrosion resistance. The EIS data were analyzed using Nyquist and Bode plots. The impedance is a complex quantity comprising a real Z' and an imaginary component Z''. The Nyquist plots revealed the existence of a capacitive loop at high frequencies and an inductive loop at low frequencies, indicating the effectiveness of the modified h-BN nanosheets in reducing corrosion. The system's behavior was examined using EIS tests performed at room temperature on BN-coated steel samples to determine linearity, causality, and durability [34]. Figure 8d illustrates a circuit compatible with the Nyquist diagram. The phosphate coatings prepared at 45 °C exhibited the highest polarization resistance, as evident from Table 1. Additionally, they demonstrated the most negligible corrosion current density. These favorable outcomes can be attributed to the more compact and condensed structure of the coating. It was reported that the formation of phosphophyllite was increased due to a slow reaction during zinc phosphating [35]. While high temperatures increase the reaction rate, they also reduce the amount of phosphophyllite phase.

It has been suggested that a temperature rise can result in an increased rate of metal dissolution, leading to large crystal formations. Furthermore, high temperatures result in a high conversion of soluble zinc phosphate to insoluble tertiary zinc phosphate and free phosphoric acid [36]. This transformation could detrimentally affect the coating, resulting in more refined crystals with heavy coating deposition and decreased corrosion [12].

The results of the fitting process are displayed in Table 2, using an EEC with a model of $R(Q(R(QR)))$ for simulating the studied interface. This model included five components, as shown in Figure 8d. This circuit consists of a solution resistance (R_s) and a charge transfer resistance (R_{ct}). It includes a phase element referred to as coating capacitance (CPE_c) in parallel with the resistance of the ionic current flowing through the coating (R_c). The high-frequency region of the model is resolved based on the intrinsic properties of the coating, including coating thickness, quantities, and pitholes. Its final part comprises a second constant phase element labeled double-layer capacitance (CPE_{dl}) and the parallel charge transfer resistance (R_{ct}). The impedance of the CPE to the dispersion can be expressed by $Z = [Y(j\omega)n]^{-1}$, where Z is the CPE's impedance and Y and n represent a coefficient ranging from 0–1 and the interfacial capacitance, respectively. j is an imaginary number, and ω is the angular frequency with the maximum imaginary impedance [10]. Table 2 shows higher corrosion resistance in the S-45 sample. It is because the more uniform phosphate coating on the surface leads to a decline in the active area of the substrate.
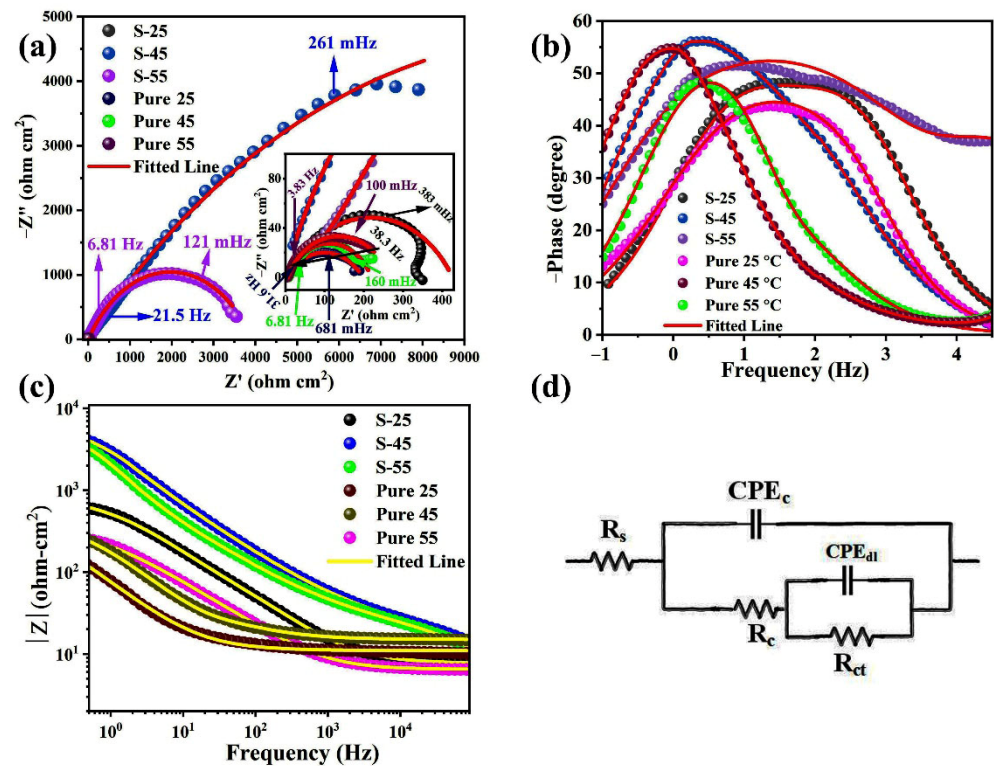
Figure 8. EIS measurements of phosphate coating samples at different temperatures (25 °C, 45 °C, and 55 °C, respectively). (**a**) Nyquist plots; (**b**) Phase angle plots; (**c**) Bode plots; and (**d**) equivalent circuit diagrams.

Table 2. Electrochemical parameters based on the circuit.

Sample	R_s ($\Omega \cdot cm^2$)	CPE_c Y_o ($\Omega^{-1} \cdot cm^{-2} \cdot s^n$)	n	R_c ($\Omega \cdot cm^2$)	CPE_{dl} Y_o ($\Omega^{-1} \cdot cm^{-2} \cdot s^n$)	n	R_{ct} ($\Omega \cdot cm^2$)
Pure 25 (25 °C)	6.47	3.57×10^{-3}	0.72	19.3	1.87×10^{-4}	0.68	361.5
Pure 45 (45 °C)	15.01	2.64×10^{-4}	0.69	28.73	9.04×10^{-4}	0.54	519.9
Pure 55 (55 °C)	10.97	3.57×10^{-3}	0.77	27.86	2.41×10^{-4}	0.65	396.9
S-25 (25 °C)	7.63	1.57×10^{-4}	0.73	123.2	2.06×10^{-4}	0.66	692.9
S-45 (45 °C)	1.02	1.53×10^{-7}	0.82	2433	4.63×10^{-6}	0.78	4621
S-55 (55 °C)	20.51	4.93×10^{-6}	0.64	287.4	9.36×10^{-6}	0.62	7808

4. Conclusions

This study investigated the effect of temperature on the morphology and corrosion resistance of modified boron nitride nanosheets incorporated into steel phosphate coatings. The results indicate that the anodic and cathodic currents declined while the polarization resistance increased after the exposure of S-25, S-45, and S-55 samples to varying immersion temperatures. In addition, scanning electron microscopy revealed that S-45 steel samples achieve denser and more uniform coatings with enhanced corrosion resistance performance compared to S-25 and S-55 steel samples. The potentiodynamic polarization results indicate that the S-45 steel specimen displayed superior corrosion resistance performance, with an electric current density of 5.48×10^{-8} A/cm^2, one order of magnitude lower than that of the S-25 and S-55 specimens, respectively. Based on the coating weight analysis, it was determined that the S-45 steel sample exhibited the highest coating density and uniformity, with a value of 32.14 g/m^2.

References

1. Tarka, K.; Jaako, A.; Persson, D.; Mattsson, H.; Johansson, L.-G. Corrosion Propagation Under Paint Films on Galvanized Steel: A Comparison of Phosphating and Thin Film Corrosion Pretreatment Technologies. In *Sustainable Automotive Technologies 2014*; Springer International Publishing: Cham, Switzerland, 2015; pp. 163–170. [CrossRef]
2. Amirudin, A.; Thierry, D. Corrosion mechanisms of phosphated zinc layers on steel as substrates for automotive coatings. *Prog. Org. Coat.* **1996**, *28*, 59–75. [CrossRef]
3. Gao, Z.; Zhang, D.; Li, X.; Jiang, S.; Zhang, Q. Current status, opportunities and challenges in chemical conversion coatings for zinc. *Colloids Surf. A Physicochem. Eng. Asp.* **2018**, *546*, 221–236. [CrossRef]
4. Simescu, F.; Idrissi, H. Corrosion behaviour in alkaline medium of zinc phosphate coated steel obtained by cathodic electrochemical treatment. *Corros. Sci.* **2009**, *51*, 833–840. [CrossRef]
5. Abdalla, K.; Azmi, R.; Azizan, A. The Influence of Deposition Temperature on the Morphology and Corrosion Resistance of Zinc Phosphate Coating on Mild Steel. *Adv. Mater. Res.* **2012**, *626*, 183–189. [CrossRef]
6. Abbasi, M.; Attar, M.M. Effect of vanadium additive and phosphating time on anticorrosion, morphology and surface properties of ambient temperature zinc phosphate conversion coatings on mild steel. *J. Coat. Technol. Res.* **2017**, *14*, 1435–1445. [CrossRef]
7. Li, R.; Yu, Q.; Yang, C.; Chen, H.; Xie, G.; Guo, J. Innovative cleaner production for steel phosphorization using Zn–Mn phosphating solution. *J. Clean. Prod.* **2010**, *18*, 1040–1044. [CrossRef]
8. Tian, Y.; Huang, H.; Wang, H.; Xie, Y.; Sheng, X.; Zhong, L.; Zhang, X. Accelerated formation of zinc phosphate coatings with enhanced corrosion resistance on carbon steel by introducing α-zirconium phosphate. *J. Alloys Compd.* **2020**, *831*, 154906. [CrossRef]
9. Fouladi, M.; Amadeh, A. Effect of phosphating time and temperature on microstructure and corrosion behavior of magnesium phosphate coating. *Electrochim. Acta* **2013**, *106*, 1–12. [CrossRef]
10. Muhammad, M.; Hu, S.; Ma, R.; Du, A.; Wang, M.; Fan, Y.; Zhao, X.; Yang, H.; Li, C.C.; Cao, X. Enhancing the corrosion resistance of Q235 mild steel by incorporating poly(dopamine) modified h-BN nanosheets on zinc phosphate-silane coating. *Surf. Coat. Technol.* **2020**, *390*, 125682. [CrossRef]
11. Narayanan, T.S.N.S.; Jegannathan, S.; Ravichandran, K. Corrosion resistance of phosphate coatings obtained by cathodic electrochemical treatment: Role of anode–graphite versus steel. *Prog. Org. Coat.* **2006**, *55*, 355–362. [CrossRef]
12. Asadi, V.; Danaee, I.; Eskandari, H. The Effect of Immersion Time and Immersion Temperature on the Corrosion Behavior of Zinc Phosphate Conversion Coatings on Carbon Steel. *Mater. Res.* **2015**, *18*, 706–713. [CrossRef]
13. Zhang, D. Preparation of Zn-Ca Phosphate Coating in Presence of PTFE on 45 Steel and its Corrosion Properties in Simulated Seawater. *Int. J. Electrochem. Sci.* **2022**, *17*, 220947. [CrossRef]
14. Xie, Y.; Chen, M.; Xie, D.; Zhong, L.; Zhang, X. A fast, low temperature zinc phosphate coating on steel accelerated by graphene oxide. *Corros. Sci.* **2017**, *128*, 1–8. [CrossRef]
15. Shibli, S.M.A.; Chacko, F. Development of nano TiO2-incorporated phosphate coatings on hot dip zinc surface for good paintability and corrosion resistance. *Appl. Surf. Sci.* **2011**, *257*, 3111–3117. [CrossRef]
16. Arthanareeswari, M.; Kamaraj, P.; Tamilselvi, M.; Devikala, S. A low temperature nano TiO 2 incorporated nano zinc phosphate coating on mild steel with enhanced corrosion resistance. *Mater. Today Proc.* **2018**, *5*, 9012–9025. [CrossRef]
17. Huang, H.; Wang, H.; Xie, Y.; Dong, D.; Jiang, X.; Zhang, X. Incorporation of boron nitride nanosheets in zinc phosphate coatings on mild steel to enhance corrosion resistance. *Surf. Coat. Technol.* **2019**, *374*, 935–943. [CrossRef]
18. Hu, S.; Muhammad, M.; Wang, M.; Ma, R.; Du, A.; Fan, Y.; Cao, X.; Zhao, X. Corrosion resistance performance of nano-MoS2-containing zinc phosphate coating on Q235 steel. *Mater. Lett.* **2020**, *265*, 127256. [CrossRef]
19. Di Giampaolo, A.R.; Medina, M.; Reyes, R.; Velez, M. Zinc phosphate interlayer for sol-gel-derived aluminosilicate coating on AISI-1010 carbon steel. *Surf. Coat. Technol.* **1997**, *89*, 31–37. [CrossRef]
20. Ding, X.; Xue, L.; Wang, X.; Ding, K.; Cui, S.; Sun, Y.; Li, M. Influence of bath PH value on microstructure and corrosion resistance of phosphate chemical conversion coating on sintered Nd–Fe–B permanent magnets. *J. Magn. Magn. Mater.* **2016**, *416*, 247–255. [CrossRef]

21. Kumari, S.; Sharma, O.P.; Gusain, R.; Mungse, H.P.; Kukrety, A.; Kumar, N.; Sugimura, H.; Khatri, O.P. Alkyl-Chain-Grafted Hexagonal Boron Nitride Nanoplatelets as Oil-Dispersible Additives for Friction and Wear Reduction. *ACS Appl. Mater. Interfaces* **2015**, *7*, 3708–3716. [CrossRef]

22. Wang, X.; Hu, W.; Hu, Y. Polydopamine-Bridged Synthesis of Ternary h-BN@PDA@TiO$_2$ as Nanoenhancers for Thermal Conductivity and Flame Retardant of Polyvinyl Alcohol. *Front. Chem.* **2020**, *8*, 587474. [CrossRef]

23. Yue, Y.-Y.; Liu, Z.-X.; Wan, T.-T.; Wang, P.-C. Effect of phosphate–silane pretreatment on the corrosion resistance and adhesive-bonded performance of the AZ31 magnesium alloys. *Prog. Org. Coat.* **2013**, *76*, 835–843. [CrossRef]

24. Sinha, P.K.; Feser, R. Phosphate coating on steel surfaces by an electrochemical method. *Surf. Coat. Technol.* **2002**, *161*, 158–168. [CrossRef]

25. Muhammad, M.; Ma, R.; Du, A.; Fan, Y.; Zhao, X.; Cao, X. Preparation and Modification of Polydopamine Boron Nitride—Titanium Dioxide Nanohybrid Particles Incorporated into Zinc Phosphating Bath to Enhance Corrosion Performance of Zinc Phosphate-Silane Coated Q235 Steel. *Materials* **2023**, *16*, 3835. [CrossRef]

26. Wang, Y.; Shi, Z.; Yin, J. Boron nitride nanosheets: Large-scale exfoliation in methanesulfonic acid and their composites with polybenzimidazole. *J. Mater. Chem.* **2011**, *21*, 11371. [CrossRef]

27. Cui, M.; Ren, S.; Qin, S.; Xue, Q.; Zhao, H.; Wang, L. Processable poly(2-butylaniline)/hexagonal boron nitride nanohybrids for synergetic anticorrosive reinforcement of epoxy coating. *Corros. Sci.* **2018**, *131*, 187–198. [CrossRef]

28. Zhi, C.; Bando, Y.; Tang, C.; Kuwahara, H.; Golberg, D. Large-Scale Fabrication of Boron Nitride Nanosheets and Their Utilization in Polymeric Composites with Improved Thermal and Mechanical Properties. *Adv. Mater.* **2009**, *21*, 2889–2893. [CrossRef]

29. Li, G.; Xing, R.; Geng, P.; Liu, Z.; He, L.; Wang, N.; Zhang, Q.; Qu, X. Surface modification of boron nitride via poly (dopamine) coating and preparation of acrylonitrile-butadiene-styrene copolymer/boron nitride composites with enhanced thermal conductivity. *Polym. Adv. Technol.* **2018**, *29*, 337–346. [CrossRef]

30. Xie, B.-H.; Huang, X.; Zhang, G.-J. High thermal conductive polyvinyl alcohol composites with hexagonal boron nitride microplatelets as fillers. *Compos. Sci. Technol.* **2013**, *85*, 98–103. [CrossRef]

31. Narayanan, T.S.N.S.; Subbaiyan, M. Overheating—Its decisive role in phosphating. *Met. Finish.* **1995**, *93*, 30–31. [CrossRef]

32. Narayanan, T.S.N.S. Surface pretreatment by phosphate conversion coatings—A review. *Rev. Adv. Mater. Sci.* **2005**, *9*, 130–177.

33. Liu, B.; Zhang, X.; Xiao, G.; Lu, Y. Phosphate chemical conversion coatings on metallic substrates for biomedical application: A review. *Mater. Sci. Eng. C* **2015**, *47*, 97–104. [CrossRef]

34. Tamilselvi, M.; Kamaraj, P.; Arthanareeswari, M.; Devikala, S. Nano zinc phosphate coatings for enhanced corrosion resistance of mild steel. *Appl. Surf. Sci.* **2015**, *327*, 218–225. [CrossRef]

35. Ashassi-Sorkhabi, H.; Seifzadeh, D.; Harrafi, H. Phosphatation of iron powder metallurgical samples for corrosion protection. *J. Iran. Chem. Soc.* **2007**, *4*, 72–77. [CrossRef]

36. Jegannathan, S.; Narayanan, T.S.N.S.; Ravichandran, K.; Rajeswari, S. Evaluation of the corrosion resistance of phosphate coatings obtained by anodic electrochemical treatment. *Prog. Org. Coat.* **2006**, *57*, 392–399. [CrossRef]